

Suppressing the loss of ultracold molecules via the continuous quantum Zeno effect

B. Zhu¹, B. Gadway¹, M. Foss-Feig², J. Schachenmayer¹, M. L. Wall¹, K. R. A. Hazzard¹,

B. Yan¹, S. A. Moses¹, J. P. Covey¹, D. S. Jin¹, J. Ye¹, M. Holland¹, A. M. Rey^{1*}

¹JILA, NIST, Department of Physics, University of Colorado, 440 UCB, Boulder, CO 80309, USA and

²JQI, NIST, Department of Physics, University of Maryland, College Park, MD 20742, USA

(Dated: July 17, 2022)

We develop theoretical methods that describe suppression of two-body losses when they are larger than all other energy scales in a lattice. These methods are necessary to explain recently observed suppression of chemical reactions between two rotational states of fermionic KRb molecules confined in one-dimensional tubes with a weak lattice along the tubes [Yan *et al.* Nature 501, 521-525 (2013)]. There, the loss suppression was attributed to the combined effects of lattice confinement and the continuous quantum Zeno effect. While a single-band theory qualitatively describes the data, quantitative analysis was not possible before because the on-site loss rate is larger than the band gap. Here, we derive a renormalized single-band model which accounts for three-dimensional multi-band effects and formulate from it a simplified rate equation and mean-field theory validated by comparing with numerically exact time-dependent density matrix renormalization group calculations. Experimental measurements performed to ensure stringent reproducibility of the initial conditions allow us to demonstrate that the renormalized model captures the measured loss rate's dependence on all lattice parameters, and enable us to quantitatively determine the filling fraction.

PACS numbers: 03.65.Xp, 67.85.-d, 37.10.Jk, 37.10.Pq

Ultracold molecules have tremendous applications ranging from quantum many-body physics [1–3] and quantum information processing [4] to precision measurements [5] and ultracold chemistry [6]. However, fast inelastic two-body losses – as occur for KRb with exothermic chemical reactions – can limit molecule lifetimes [7–9], and have been considered a fundamental limitation.

In this Letter, we show through theory and experiment that even when two-body inelastic collision rates are faster than all other rates in the system, molecules can live orders of magnitude longer than timescales for interesting coherent dynamics. The enhanced lifetime in an optical lattice is shown to be a consequence of the continuous quantum Zeno effect – the suppression of coherent transitions into strongly dissipative states [10–14]. Long lifetimes open a path to explore coherent many-body physics in highly reactive systems, even where motion in the lattice is important.

Inhibition of losses by strong dissipation has been observed for bosonic Feshbach molecules [15] and, recently, in fermionic ground state KRb molecules [16]. To reach the regime where losses are much faster than motional rates, both experiments confined molecules in an array of one-dimensional tubes and added an axial optical lattice along the tubes (Fig. 1). The axial lattice induces an energy gap between the single-particle lowest band energy states and higher energy single-particle states. Previously, discussion of the Zeno effect has been based on the approximation that inelastic interactions do not affect the lowest band wavefunctions [14, 17]. However, this assumption strongly limits the investigation of the Zeno effect, which requires strongly dissipative systems. For example Feshbach molecules [15] exhibit loss rates comparable to the band gap of the axial lattice. KRb molecules exhibit loss rates at least five times larger [16], fully invalidating this assumption [18]. A proper description of the dissipative dynamics requires theoretical methods that non-

perturbatively include three-dimensional-multi-band modifications to the lowest band single-particle orbitals generated by inelastic collisions.

Here we develop such a theoretical description. In parallel we perform systematic measurements of the KRb lifetime under different lattice conditions. The observed dependence of the loss rate on lattice parameters is consistent with the one previously reported in Ref. [16] and fully reproduced by the theory. The theory-experiment agreement allows us to conclude that the observed inhibition of losses is a direct consequence of the quantum Zeno effect.

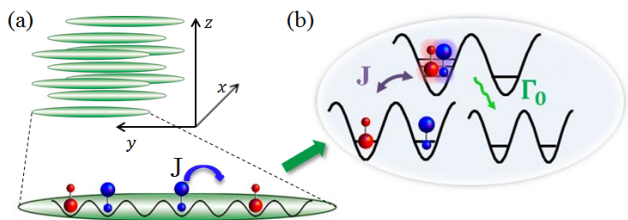


FIG. 1. (a) A 50:50 mixture of fermionic KRb molecules in two rotational states, $|0, 0\rangle$ (red) and $|1, -1\rangle$ (blue), is prepared in a deep 3D lattice, which is suddenly made shallow along one dimension (y). Along y , molecules tunnel with a rate J/\hbar and have a large on-site loss rate Γ_0 because of chemical reactions. (b) In the Zeno regime, $\hbar\Gamma_0 \gg J$, doubly occupied sites are only virtually populated, and the loss occurs at a significantly slower rate $\Gamma_{\text{eff}} \ll \Gamma_0$ for molecules on adjacent sites. For KRb, a multi-band analysis of this process is required for all experimental lattice parameters.

A major unknown in our experiment is the filling fraction of molecules, f , which crucially affects the many-body dynamics. Our improved theory, in conjunction with measurements of systems carefully prepared to have similar initial conditions (and thus a constant f) between realizations, allows a quanti-

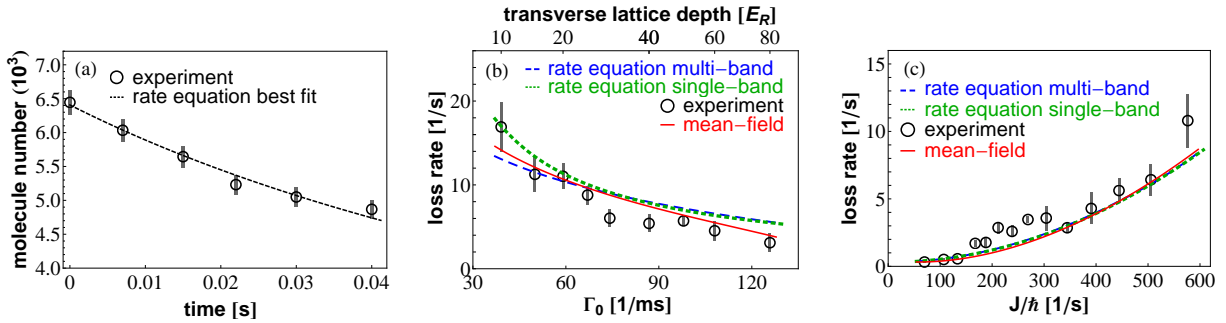


FIG. 2. (a) Measured number loss of $|\downarrow\rangle$ molecules for an axial (transverse) lattice depth of $V_y = 5 E_R$ ($V_\perp = 25 E_R$) (circles) and best fit using the rate equation (RE), Eq. (2) (black dashed line). (b) Number loss rate, κ , as a function of Γ_0 (fixing J and varying the bare on-site rate via V_\perp). (c) Number loss rate, κ , versus J for fixed Γ_0 (varying V_y and adjusting V_\perp accordingly). V_y (V_\perp) was varied from 5 to 16 E_R (20 to 40 E_R). Black circles are experimental measurements (error bars represent one standard error). Green short-dashed lines show solutions of the RE Eq. (2) using an effective loss rate Γ_{eff} (single-band approximation). Blue long-dashed and solid red lines show RE and MF theories, respectively, using Γ_{eff} (multi-band model). The MF, multi-band RE, and single-band RE theories (red, blue and green lines) were obtained by fixing the filling fraction to be $\approx 9\%$, 6% , and 25% respectively. Panels (b) and (c) directly manifest the continuous quantum Zeno effect: in (b) the measured loss rate κ decreases with increasing on-site Γ_0 ; in (c) a fit to the experimental data supports $\kappa \propto J^2$, with a χ^2 (sum of the squared fitting errors) several times smaller than that obtained fitting to $\kappa \propto J$.

tative determination of f .

After developing an effective single-band model, we use a mean-field (MF) approximation, whose accuracy we validate by comparing to a numerically exact method combining time-dependent density matrix renormalization group (t-DMRG) [19–21] with quantum trajectories [22–24]. We compare MF results with simple rate equations (REs), often used to model two-body losses. We find that although the REs capture the dynamics for a broad range of lattice parameters, the MF better reproduces the observed decay for deeper lattices, where increased harmonic confinement from the lattice lasers modifies transport during the dissipative dynamics. The MF theory reproduces all measurements of the loss rate using a single filling f , which is consistent with that extracted from Ramsey spectroscopy of molecules pinned in a 3D lattice and prepared under similar initial conditions [16, 25]. In contrast, a single-band model predicts a much larger f .

The experiment begins by loading $\sim 10^4$ fermionic KRb ro-vibrational ground state molecules, $|N = 0, m_N = 0\rangle$, into the lowest band of a deep 3D cubic optical lattice with lattice constant $a = 532$ nm. Here, N is the principal rotational quantum number and m_N is the projection onto the quantization axis, which in our case is determined by an external magnetic field angled 45° between the x and y lattice directions. We next apply a $\pi/2$ microwave pulse to rotationally excite half of the molecules to $|N = 1, m_N = -1\rangle$. We consider $|0, 0\rangle$ and $|1, -1\rangle$ as $|\downarrow\rangle$ and $|\uparrow\rangle$ components of a pseudo-spin 1/2 system. We choose the lattice polarizations so that the tensor AC polarizabilities of $|0, 0\rangle$ and $|1, -1\rangle$ are similar [26]. However, the residual differential AC Stark shift introduces single-particle dephasing, resulting in a spin-coherence time for the entire sample of ~ 1 ms. This dephasing is used to prepare a mostly incoherent 50:50 spin mixture of $|\downarrow\rangle$ and $|\uparrow\rangle$ by holding the molecules in the deep lattice for

50 ms. Losses are initiated by quickly ramping down the lattice depth in the y direction (within 1 ms) to allow tunneling. We measure the number of remaining $|\downarrow\rangle$ molecules as a function of the subsequent holding time in the lattice.

The two-body loss rate coefficient between molecules in $|0, 0\rangle$ and $|1, -1\rangle$, $\beta^{(3D)}$, was measured to be $\beta^{(3D)} = 9.0(4) \times 10^{-10} \text{ cm}^3 \text{ s}^{-1}$ [16]. In a lattice, within the single-band approximation, which assumes Wannier orbitals unperturbed by interaction effects, the on-site bare loss rate Γ_0 is [14]

$$\Gamma_0 = \beta^{(3D)} \int |W(\mathbf{x})|^4 d^3x, \quad (1)$$

where $W(\mathbf{x})$ is the lowest-band 3D Wannier orbital (elastic on-site interactions are assumed much smaller, and negligible). Furthermore, although a transition dipole matrix element exists between $|\uparrow\rangle$ and $|\downarrow\rangle$, we neglect dipolar interactions because of the lack of spin coherence in our 50:50 mixture.

From Eq. (1), one obtains $\hbar\Gamma_0/J > 60$, with J the tunneling energy between neighboring lattice sites along y , for all experimental lattice depths. A simple way to understand the Zeno mechanism is to consider two opposite spin particles, $|\uparrow, \downarrow\rangle$. Left and right sides in this notation represent left and right wells [Fig. 1(b)]. When two molecules occupy the same site only the singlet component decays (with rate Γ_0), the decay of the triplet component being suppressed by the centrifugal barrier in odd partial-wave channels [9]. Consequently, the loss rate is determined by $J_s = \sqrt{2}J$, the tunneling computed after projecting the initial wavefunction into the singlet state $|s\rangle = (|\uparrow, \downarrow\rangle - |\downarrow, \uparrow\rangle)/\sqrt{2}$. When $\hbar\Gamma_0 \gg J_s$, second-order perturbation theory can be applied and gives a net $|\downarrow\rangle$ loss rate of $4\Gamma_{\text{eff}}$ with $\Gamma_{\text{eff}} = \frac{2(J/\hbar)^2}{\Gamma_0}$.

The prior loss-rate can be connected to number loss dynamics with a rate equation (RE), $\frac{dn_{j,\downarrow}}{dt} = -qXn_{j+1,\uparrow}n_{j,\downarrow}$,

where $n_{j,\downarrow}$ is the number of $|\downarrow\rangle$ molecules at site j and q is the number of nearest neighbors ($q = 2$ for tunneling along the tube direction) [17]. The number of adjacent $|\uparrow\rangle$ molecules is on average $qn_{j+1,\uparrow}$ and $X = 4\Gamma_{\text{eff}}$ is the loss rate of a $|\downarrow\rangle$ molecule due to neighboring $|\uparrow\rangle$ molecules. Assuming a uniform distribution, the 50:50 mixture implies $n_{j+1,\uparrow} = n_{j,\downarrow} = n_\downarrow$ and

$$\frac{dn_\downarrow}{dt} = -8\Gamma_{\text{eff}}n_\downarrow(t)^2 \quad \text{or} \quad \frac{dN_\downarrow}{dt} = -\frac{\kappa}{N_\downarrow(0)}N_\downarrow(t)^2, \quad (2)$$

where $\kappa = 8\Gamma_{\text{eff}}n_\downarrow(0)$ and $N_\downarrow(t)$ is the number of $|\downarrow\rangle$ molecules. The filling fraction $f = 2n_\downarrow(0)$. The RE should be valid at short times and when f determines the losses (generally true for $J \gg \Gamma_{\text{eff}}$).

To determine the applicability of the RE, we perform new measurements of the loss rate κ 's dependence on Γ_0 and J for fixed f . Ref. [16] performed similar measurements, however here we ensure stringent reproducibility of initial conditions (to fix f) for all lattice conditions. We determine κ by measuring $N_\downarrow(t)$ and fitting this loss curve to the solution of Eq. (2) [Fig. 2(a)]. We measure the Γ_0 -dependence by setting $V_y = 5E_R$, which fixes J , and then tuning Γ_0 by modifying V_\perp [Fig. 2(b)]. Here, $E_R = \hbar^2\pi^2/2ma^2$ is the recoil energy and m is the KRb mass. To study the J -dependence, we vary V_y while simultaneously adjusting V_\perp to keep Γ_0 fixed [Fig. 2(c)]. The loss rate κ depends quadratically on J for fixed Γ_0 and decreases with increasing Γ_0 for fixed J , as expected from the single-band model.

All parameters are known except f . In order to fit the experiment, the single-band RE [green-short-dashed line in Figs. 2(b)-(c)] requires $f \approx 25\%$, inconsistent with $f \lesssim 10\%$ estimated by a cluster expansion comparison to the Ramsey fringe contrast decay in the experiment of Ref. [16]. It is also inconsistent with prior estimates from loss rate measurements in a gas of identical molecules [27] and from *in situ* measurements of the density. Resolution of this discrepancy requires a proper treatment of (i) mixing of higher bands and (ii) molecule redistribution during the dynamics, both of which will now be addressed.

As shown in the Supplementary Material, a single-band model overestimates Γ_0 , predicting it to be larger than the band gap. Incorporating higher bands decreases Γ_0 and hence decreases the estimated f (since the effective loss rate is inversely proportional to Γ_0). We extract a renormalized effective loss rate by numerically computing loss for two molecules trapped in a double well along y . We expand the non-Hermitian Hamiltonian $\hat{H} = \hat{H}_0 - i\hbar\beta^{(3D)}\delta_{\text{reg}}(\mathbf{r})/2$, where $\delta_{\text{reg}}(\mathbf{r}) = \delta(\mathbf{r})(\partial/\partial r)r$ is a regularized pseudopotential [28] and \hat{H}_0 the single-particle Hamiltonian, in the 3D Wannier function basis. This model accounts for interaction-mediated band excitations in all three dimensions. We initialize the system with two molecules in the singlet $|s\rangle$ and infer the effective loss rate by fitting the norm decay to $\exp(-4\tilde{\Gamma}_{\text{eff}}t)$. Convergence is achieved with ~ 6 bands in each dimension.

The computed $\tilde{\Gamma}_{\text{eff}}$ is ~ 5 times larger than Γ_{eff} ; however, both exhibit a similar power-law dependence on V_\perp ($\tilde{\Gamma}_{\text{eff}}/\Gamma_{\text{eff}} \propto V_\perp^{0.16}$) and scale quadratically with J . This is demonstrated in Fig. 2(b)-(c), which shows the single-band (green-short-dashed lines) and multi-band (blue-long-dashed lines) solutions. The latter is obtained by substituting $\Gamma_{\text{eff}} \rightarrow \tilde{\Gamma}_{\text{eff}}$ in Eq. (2) and using $f = 5.6\%$, roughly five times smaller than that used for the single-band calculation. The RE describes the experimental observations fairly well at intermediate V_\perp but deviates from them for the largest V_\perp . We attribute these deviations to the suppression of tunneling at the cloud's edges due to the energy mismatch between adjacent sites in the harmonic potential generated by the lattice beams. This effect is relevant for the largest V_\perp , where it causes the decay rate to depend on the molecule distribution at each time, and cannot be captured by the RE.

We can simultaneously account for dynamical redistribution of molecules and multi-band effects by solving a single-band master equation with a density matrix, $\hat{\rho}$, projected into the states with at most one molecule per site after adiabatic elimination of doubly occupied states. We keep terms up to order Γ_{eff} [14], replace the single-band Γ_{eff} by the renormalized loss rate extracted from the multi-band double well solution, and obtain

$$\frac{d}{dt}\hat{\rho} = -\frac{i}{\hbar}[\hat{H}_0, \hat{\rho}] + \mathcal{L}\hat{\rho}, \quad (3)$$

with $\hat{H}_0 = -J\sum_{j,\sigma}(\hat{c}_{\sigma j}^\dagger\hat{c}_{\sigma j+1} + h.c.) + \sum_{j,\sigma}V_j^\sigma\hat{c}_{\sigma j}^\dagger\hat{c}_{\sigma j}$ and $\mathcal{L}\hat{\rho} = \frac{1}{2}\sum_j[2\hat{A}_j\hat{\rho}\hat{A}_j^\dagger - \hat{\rho}\hat{A}_j^\dagger\hat{A}_j - \hat{A}_j^\dagger\hat{A}_j\hat{\rho}]$ [29]. Here, $V_j^\sigma = \frac{1}{2}m\omega_\sigma^2j^2a^2$ is the parabolic trapping potential felt by molecules in state σ at site j . The average trap frequency $(\omega_\uparrow + \omega_\downarrow)/2$ varies between $\approx 2\pi \times (15 - 40)$ Hz for the experimental range of V_\perp . The σ -dependence is due to residual differential AC Stark shifts between the two rotational states. \mathcal{L} is a Lindblad superoperator that accounts for losses, and the jump operators are $\hat{A}_j = \sqrt{2\tilde{\Gamma}_{\text{eff}}}[(\hat{c}_{j\uparrow}\hat{c}_{j+1\downarrow} + \hat{c}_{j\uparrow}\hat{c}_{j-1\downarrow}) - (\hat{c}_{j\downarrow}\hat{c}_{j+1\uparrow} + \hat{c}_{j\downarrow}\hat{c}_{j-1\uparrow})]$. We checked the validity of the renormalized single-band model by confirming that it reproduces the dynamics of the multi-band problem for the case of two molecules in four wells.

To solve Eq. (3) we map the hardcore fermions onto hardcore spin-1/2 bosons [30], and then use a MF ansatz $\hat{\rho} = \prod_j\tilde{\rho}_j$ with $\tilde{\rho}_j = \sum_{\alpha,\beta=\{\uparrow,\downarrow,0\}}\rho_j^{\alpha,\beta}| \alpha \rangle \langle \beta |$. Here, $\tilde{\rho}_j$ is the reduced projected density matrix at site j , and $\uparrow, \downarrow, 0$ label the three possible local states of spin up, down, and the vacuum, respectively. This ansatz leads to closed equations of motion for $\rho_j^{\alpha,\beta}$ (see Supplementary Material), which simplify further since here $\rho_j^{\sigma,\sigma'} = 0$ for an incoherent spin mixture. Although the mean-field treatment predicts no coherent tunneling for a pure Fock state, we initiate it by assuming non-zero particle/hole coherence $|\rho_j^{\sigma,0}| = 1/2$.

We assume that molecules are initially uniformly distributed within a shell with inner (outer) radius of 20 (50) lat-

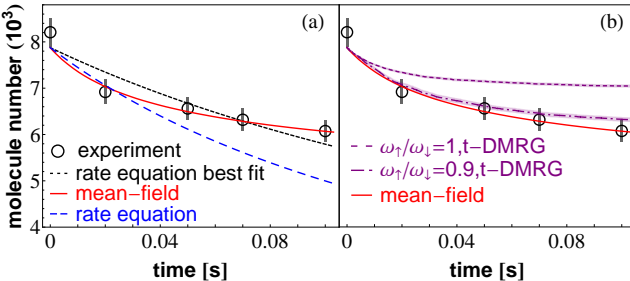


FIG. 3. Comparison of experimental loss dynamics for the deepest considered lattice to MF and t-DMRG calculations. (a) Molecule loss vs. time for $V_{\perp} = 80 E_R$ and $V_y = 5 E_R$ [Identical conventions/conditions to Fig. 2(b)]. The MF matches the experimental data better than the REs. (b) Comparison of t-DMRG simulations ($\chi_{\text{mps}} = 128$, 2000 trajectories) to MF, for two different cases: i) an identical trap for the two spin states with trap frequency $\omega_{\perp} = \omega_{\uparrow} = 2\pi \times 38$ Hz; and ii) slightly different trap frequencies $\omega_{\perp} = 2\pi \times 38$ Hz, $\omega_{\uparrow} = 2\pi \times 34.2$ Hz. Shaded areas indicate the standard error of the mean.

tice sites. The shell distribution is expected because molecules are created from a Mott insulator of Rb and a band insulator of K. Assuming only sites with one Rb and one K can yield molecules during STIRAP [7, 27], sites in the trap center initially doubly occupied by Rb atoms are lost [7]. We average over random initial configurations, since the experiments measure an ensemble of 1D tubes.

The MF assumption is an extreme approximation precluding entanglement between parts of the system. In order to test its validity, we also solve Eq. (3) numerically by combining t-DMRG algorithms [19–21] with a stochastic sampling over quantum trajectories [22–24, 31]. The results (Fig. 3) are converged in the matrix product state dimension χ_{mps} and therefore numerically exact. Fig. 3(a) shows the dynamics for the largest V_{\perp} ; here, the RE fails to properly describe the dynamics. Even though molecule redistribution due to coherent tunneling is playing an important role in the dynamics, t-DMRG and MF solutions agree within the experimental error bars up to a decay of $\sim 20\%$ in the particle number (the typical range used to extract loss rates from the data) [Fig. 3 (b)]. The deviations between t-DMRG and MF for the longest molecule lifetimes (largest V_{\perp}) and identical traps show that non-trivial correlations (manifested as loss saturation) can be generated during the dynamics [32].

With the validity of the MF established, we use it to model the experiment. Figures 2 (b-c) show the MF results (red line) and the renormalized RE (dashed blue line). We use fillings $f = 8.7\%$ and $f = 5.6\%$, respectively, to match the experiment. The extracted MF f is slightly larger than that from the RE since the latter overestimates the loss rate [Figs. 2(a)-(b)]. However, the initial molecule distribution is only approximately known, introducing uncertainty in the estimated f primarily for the deeper lattices where the dynamics are geometry dependent. Varying the shell width yields $f \sim 9 \pm 2\%$.

Although the RE captures much of the observed dependence, the MF accounts better for the inhibition of losses observed in deep lattices. Deviations are seen only for the shallowest lattice depths, where the transverse tunneling rate is only three times smaller than the axial one, which may indicate the breakdown of 1D dynamics.

The understanding of losses gained in this work highlights the importance of band mixing for describing cold atom quantum simulators [18, 33, 34], and opens the path for laboratory explorations of iconic models of quantum magnetism combining motional and spin degrees of freedom, such as extended t - J models. These are predicted to exhibit itinerant ferromagnetism, d -wave superfluidity [35, 36], and topological phases [3, 37]. Our results also extend to other dissipative systems, such as alkaline earth atoms [38–41] and other chemically reactive molecular species [42].

Acknowledgements: The authors thank A. Daley for useful discussions and acknowledge funding from NIST, JILA-NSF-PFC, NSF-PIF, ARO, ARO-DARPA-OLE, and AFOSR. K.R.A.H., B.G. and M.F.-F. thank the NRC postdoctoral fellowship program for support. S.A.M. and J.P.C. acknowledge funding from NDSEG. A.M.R. and K.R.A.H. thank the KITP for its hospitality. This work utilized the Janus supercomputer, supported by NSF, NCAR and CU.

* arey@jila1.colorado.edu

- [1] C. Trefzger, C. Menotti, B. Capogrosso-Sansone, and M. Lewenstein, *J. Phys. B: At, Mol. Opt. Phys.* **44**, 193001 (2011).
- [2] M. Baranov, M. Dalmonte, G. Pupillo, and P. Zoller, *Chem. Rev.* **112**, 5012 (2012).
- [3] T. Lahaye, C. Menotti, L. Santos, M. Lewenstein, and T. Pfau, *Rep. Prog. Phys.* **72**, 126401 (2009).
- [4] D. DeMille, *Phys. Rev. Lett.* **88**, 067901 (2002).
- [5] T. Zelevinsky, S. Kotochigova, and J. Ye, *Phys. Rev. Lett.* **100**, 043201 (2008).
- [6] L. D. Carr, D. DeMille, R. V. Krems, and J. Ye, *New J. Phys.* **11**, 055049 (2009).
- [7] S. Ospelkaus, K.-K. Ni, D. Wang, M. De Miranda, B. Neyenhuis, G. Quéméner, P. Julienne, J. Bohn, D. S. Jin, and J. Ye, *Science* **327**, 853 (2010).
- [8] K.-K. Ni, S. Ospelkaus, D. Wang, G. Quéméner, B. Neyenhuis, M. De Miranda, J. Bohn, J. Ye, and D. S. Jin, *Nature* **464**, 1324 (2010).
- [9] M. De Miranda, A. Chotia, B. Neyenhuis, D. Wang, G. Quéméner, S. Ospelkaus, J. Bohn, J. Ye, and D. S. Jin, *Nature Phys.* **7**, 502 (2011).
- [10] B. Misra and E. C. G. Sudarshan, *J. Math. Phys.* **18**, 756 (1977).
- [11] W. M. Itano, D. J. Heinzen, J. J. Bollinger, and D. J. Wineland, *Phys. Rev. A* **41**, 2295 (1990).
- [12] M. C. Fischer, B. Gutiérrez-Medina, and M. G. Raizen, *Phys. Rev. Lett.* **87**, 040402 (2001).
- [13] Y.-J. Han, Y.-H. Chan, W. Yi, A. J. Daley, S. Diehl, P. Zoller, and L.-M. Duan, *Phys. Rev. Lett.* **103**, 070404 (2009).
- [14] J. J. García-Ripoll, S. Dürr, N. Syassen, D. Bauer, M. Lettner, G. Rempe, and J. Cirac, *New J. Phys.* **11**, 013053 (2009).
- [15] N. Syassen, D. Bauer, M. Lettner, T. Volz, D. Dietze, J. García-

- Ripoll, J. Cirac, G. Rempe, and S. Dürr, Science **320**, 1329 (2008).
- [16] B. Yan, S. A. Moses, B. Gadway, J. P. Covey, K. R. Hazzard, A. M. Rey, D. S. Jin, and J. Ye, Nature **501**, 521 (2013).
- [17] S. K. Baur and E. J. Mueller, Phys. Rev. A **82**, 023626 (2010). (We note that in this reference there is a factor of 2 missing on the right hand side of Eq. (13)).
- [18] M. J. Mark, E. Haller, K. Lauber, J. G. Danzl, A. J. Daley, and H.-C. Nägerl, Phys. Rev. Lett. **107**, 175301 (2011).
- [19] G. Vidal, Phys. Rev. Lett. **93**, 040502 (2004).
- [20] A. J. Daley, C. Kollath, U. Schollwöck, and G. Vidal, J. Stat. Mech. Theor. Exp. p. P04005 (2004).
- [21] S. R. White and A. E. Feiguin, Phys. Rev. Lett. **93**, 076401 (2004).
- [22] H. Carmichael, *An Open Systems Approach to Quantum Optics, Lectures Presented at the Université Libre de Bruxelles*, Lecture Notes in Physics monographs (Springer, 1991).
- [23] K. Mølmer, Y. Castin, and J. Dalibard, J. Opt. Soc. Am. B **10**, 524 (1993).
- [24] R. Dum, A. S. Parkins, P. Zoller, and C. W. Gardiner, Phys. Rev. A **46**, 4382 (1992).
- [25] K. R. A. Hazzard, S. R. Manmana, M. Foss-Feig, and A. M. Rey, Phys. Rev. Lett. **110**, 075301 (2013).
- [26] B. Neyenhuis, B. Yan, S. A. Moses, J. P. Covey, A. Chotia, A. Petrov, S. Kotochigova, J. Ye, and D. S. Jin, Phys. Rev. Lett. **109**, 230403 (2012).
- [27] A. Chotia, B. Neyenhuis, S. A. Moses, B. Yan, J. P. Covey, M. Foss-Feig, A. M. Rey, D. S. Jin, and J. Ye, Phys. Rev. Lett. **108**, 080405 (2012).
- [28] K. Huang and C. N. Yang, Phys. Rev. **105**, 767 (1957).
- [29] Note: The sums run over all lattice sites, operators acting outside the bounds are implicitly ignored.
- [30] H. Tsunetsugu, M. Sigrist, and K. Ueda, Rev. Mod. Phys. **69**, 809 (1997).
- [31] J. Schachenmayer, L. Pollet, M. Troyer, and A. J. Daley, arXiv: 1305.1301 (2013).
- [32] M. Foss-Feig, A. J. Daley, J. K. Thompson, and A. M. Rey, Phys. Rev. Lett. **109**, 230501 (2012).
- [33] S. Will, T. Best, U. Schneider, L. Hackermüller, D.-S. Lühmann, and I. Bloch, Nature **465**, 197 (2010).
- [34] P. Soltan-Panahi, D.-S. Lühmann, J. Struck, P. Windpassinger, and K. Sengstock, Nature Phys. **8**, 71 (2011).
- [35] A. Gorshkov, M. Hermele, V. Gurarie, C. Xu, P. Julienne, J. Ye, P. Zoller, E. Demler, M. Lukin, and A. Rey, Nature Phys. **6**, 289 (2010).
- [36] K. A. Kuns, A. M. Rey, and A. V. Gorshkov, Phys. Rev. A **84**, 063639 (2011).
- [37] M. A. Baranov, K. Osterloh, and M. Lewenstein, Phys. Rev. Lett. **94**, 070404 (2005).
- [38] A. D. Ludlow, N. D. Lemke, J. A. Sherman, C. W. Oates, G. Quéméner, J. von Stecher, and A. M. Rey, Phys. Rev. A **84**, 052724 (2011).
- [39] M. Bishop, M. J. Martin, M. D. Swallows, C. Benko, Y. Lin, G. Quéméner, A. M. Rey, and J. Ye, Phys. Rev. A **84**, 052716 (2011).
- [40] A. Traverso, R. Chakraborty, Y. N. Martinez de Escobar, P. G. Mickelson, S. B. Nagel, M. Yan, and T. C. Killian, Phys. Rev. A **79**, 060702 (2009).
- [41] C. Lisdat, J. S. R. V. Winfred, T. Middelmann, F. Riehle, and U. Sterr, Phys. Rev. Lett. **103**, 090801 (2009).
- [42] P. S. Żuchowski and J. M. Hutson, Phys. Rev. A **81**, 060703 (2010).
- [43] T. Busch, B.-G. Englert, K. Rzażewski, and M. Wilkens, Found. Phys. **28**, 549 (1998).

SUPPLEMENTARY MATERIAL

Mean-field master equation

With the procedures described in the main text, the mean-field master equation for two-component fermions with double occupancy disallowed is translated into that for two-component hard core bosons. Under the mean-field ansatz given in the text, the master equation becomes 9 coupled differential equations, which can be numerically solved efficiently for a moderate size lattice:

$$\frac{d\rho_j^{\sigma\sigma}}{dt} = iJ \sum_l (\rho_l^{\sigma 0} \rho_j^{0\sigma} - \rho_l^{0\sigma} \rho_j^{\sigma 0}) + 2\tilde{\Gamma}_{\text{eff}} \sum_l (\rho_l^{\sigma'\sigma} \rho_j^{\sigma\sigma'} + \rho_l^{\sigma\sigma'} \rho_j^{\sigma'\sigma}) - 4\tilde{\Gamma}_{\text{eff}} \sum_l \rho_l^{\sigma'\sigma'} \rho_j^{\sigma\sigma}, \quad (4)$$

$$\frac{d\rho_j^{\sigma\sigma'}}{dt} = i(\Omega_\sigma - \Omega_{\sigma'}) j^2 \rho_j^{\sigma\sigma'} + iJ \sum_l (\rho_l^{\sigma 0} \rho_j^{0\sigma'} - \rho_l^{0\sigma'} \rho_j^{\sigma 0}) + 2\tilde{\Gamma}_{\text{eff}} \sum_l \sum_\alpha (\rho_l^{\sigma\sigma'} \rho_j^{0\alpha} - \rho_l^{\alpha\alpha} \rho_j^{\sigma\sigma'}), \quad (5)$$

$$\frac{d\rho_j^{0\sigma}}{dt} = i\Omega_\sigma j^2 \rho_j^{0\sigma} + iJ \sum_l (\sum_\alpha \rho_l^{0\alpha} \rho_j^{\alpha\sigma} - \rho_l^{0\sigma} \rho_j^{00}) + 2\tilde{\Gamma}_{\text{eff}} \sum_l (\rho_l^{\sigma'\sigma} \rho_j^{0\sigma'} - \rho_l^{\sigma'\sigma'} \rho_j^{0\sigma}), \quad (6)$$

$$\frac{d\rho_j^{\sigma 0}}{dt} = -i\Omega_\sigma j^2 \rho_j^{\sigma 0} + iJ \sum_l (\rho_l^{\sigma 0} \rho_j^{00} - \sum_\alpha \rho_l^{\alpha 0} \rho_j^{\sigma\alpha}) + 2\tilde{\Gamma}_{\text{eff}} \sum_l (\rho_l^{\sigma\sigma'} \rho_j^{\sigma 0} - \rho_l^{\sigma'\sigma'} \rho_j^{\sigma 0}), \quad (7)$$

$$\frac{d\rho_j^{00}}{dt} = iJ \sum_l \sum_\alpha (\rho_l^{0\alpha} \rho_j^{\alpha 0} - \rho_l^{\alpha 0} \rho_j^{0\alpha}) + 4\tilde{\Gamma}_{\text{eff}} \sum_l \sum_{\alpha \neq \alpha'} \sum_{\beta \neq \beta'} (-1)^{\delta_{\alpha\beta}} \rho_l^{\alpha\beta} \rho_j^{\alpha'\beta'}, \quad (8)$$

where j is the site label, $\sigma, \alpha, \alpha', \beta, \beta' \in \{\uparrow, \downarrow\}$, $\sigma \neq \sigma'$, the summation of l is over the nearest neighbors of j , $\Omega_{\uparrow(\downarrow)} = \frac{1}{2}m\omega_{\uparrow(\downarrow)}^2 a^2$ with a the lattice spacing, and $1/\hbar$ has been used as the time unit. As can be seen from the form of the jump operator defined in the main text, when writing down the master equation there are additional terms such as $\hat{n}_{j\sigma}\hat{c}_{j+1\sigma'}^\dagger\hat{c}_{j-1\sigma'}\hat{p}$ and $\hat{c}_{j+1\sigma}^\dagger\hat{c}_{j\sigma}\hat{c}_{j\sigma'}^\dagger\hat{c}_{j-1\sigma'}\hat{p}$ generated by the Lindblad superoperator, which correspond to the correlated hopping processes involving three sites. In the above Eqs. (4)-(8), these terms have been neglected, and we have performed calculations to confirm the contributions from these terms are small for the systems we treat in this paper.

Convergence of the double-well, multi-band solution

In the main text we explained how we extracted the effective loss rate $\tilde{\Gamma}_{\text{eff}}$ from the dynamics of a singlet in a double well potential, taking into account three-dimensional band excitations. In this section we examine the convergence properties of this solution in more detail. In Fig. S1(a), we show the behavior of the on-site loss rate $\Gamma_0/2$ with the rate coefficient $\beta^{(3D)}$ in a single well of an optical lattice of depth $50E_R$. We extract this loss rate from the imaginary part of the eigenvalue of the complex single-well Hamiltonian with smallest real part. For perturbative losses, excitations to higher bands are negligible. For faster losses, the single-band calculation predicts a diverging loss rate while the multi-band calculation peaks at a finite value and then decreases with increasing loss rate. The decreasing effective loss rate with increasing $\beta^{(3D)}$ can be understood from the behavior of two particles in a isotropic harmonic trap subject to repulsive elastic interactions. In the case of elastic interactions, the interaction energy peaks when the s -wave scattering length a_s is of order the characteristic length scale of the trap a_{ho} , $a_s/a_{\text{ho}} \sim 1$. As $a_s/a_{\text{ho}} \rightarrow \infty$, the wavefunction of the full interacting eigenstate at zero relative separation goes to zero such that the interaction energy goes to zero while the total energy increases. As losses are due only to interactions, the effective loss rate hence also decreases as the onsite loss rate increases beyond a certain threshold. We find that for real interactions, our numerical results for a single well converge to the known solution for the harmonic oscillator with repulsive interactions [43], demonstrating that regularization is properly accounted for in our approach. For the two-well solution, the convergence is demonstrated in Fig. S1(b) using the loss rate β_{3D} for KRb and a fixed lattice depth $V_y = 5E_R$ for the tunneling direction. Interestingly, the same number of bands are required for essentially all transverse lattice depths $10E_R \leq V_\perp \leq 80E_R$ due to identical scaling of the band gap and the band-transferring interactions with the transverse lattice depth in the deep-lattice limit.

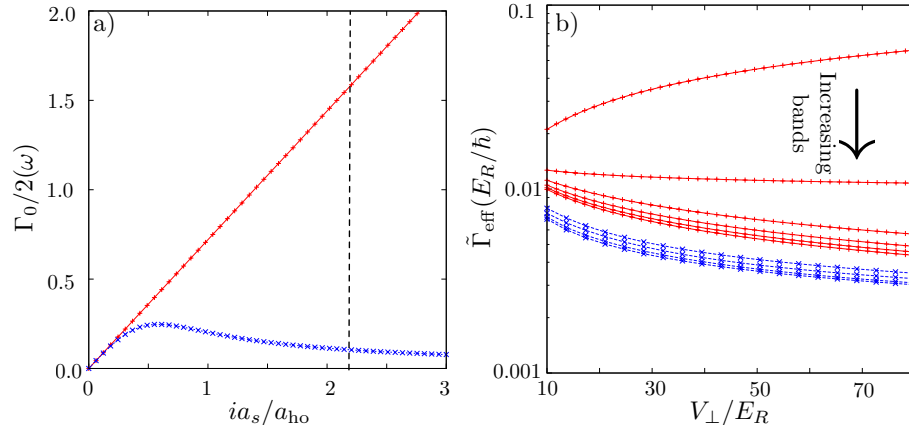


Figure S 1. (Color online) (a) The on-site loss rate in oscillator units ($\hbar\omega = 2\sqrt{VE_R}$) for two atoms in a single lattice site with depth $V = 50E_R$ is shown for a single-band calculation (solid red line) and a calculation with 6^3 bands (dashed blue line) as a function of the pure imaginary s -wave scattering length a_s in oscillator units ($a_{\text{ho}} = (a/\pi)(V/E_R)^{-1/4}$), related to the loss rate coefficient as $\beta^{(3D)} = 4\pi\hbar^2 a_s/m$. The vertical dotted line indicates the loss rate for KRb. (b) The effective loss rate of the double well calculation versus the transverse lattice height and the number of bands used in the calculation. The red solid curves use a single transverse band and 1 to 6 bands along the tunneling direction from top to bottom. The blue dashed curves use 6 bands along the tunneling direction and 3^2 to 6^2 bands along the transverse directions from top to bottom.